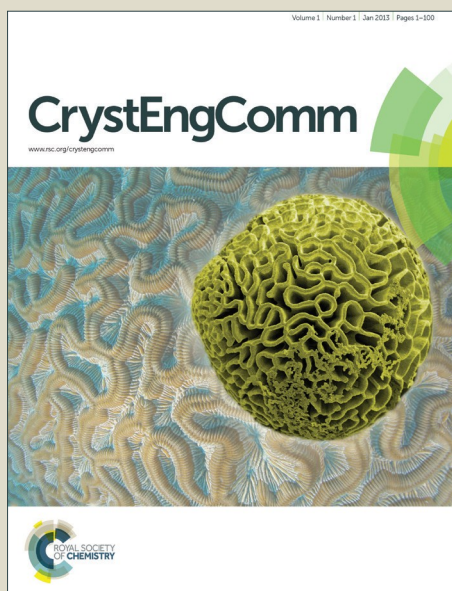


CrystEngComm

Accepted Manuscript



This article can be cited before page numbers have been issued, to do this please use: A. Pal, S. Chand, S. Senthilkumar, S. Neogi and M. C. Das, *CrystEngComm*, 2016, DOI: 10.1039/C6CE00151C.



This is an *Accepted Manuscript*, which has been through the Royal Society of Chemistry peer review process and has been accepted for publication.

Accepted Manuscripts are published online shortly after acceptance, before technical editing, formatting and proof reading. Using this free service, authors can make their results available to the community, in citable form, before we publish the edited article. We will replace this *Accepted Manuscript* with the edited and formatted *Advance Article* as soon as it is available.

You can find more information about *Accepted Manuscripts* in the [Information for Authors](#).

Please note that technical editing may introduce minor changes to the text and/or graphics, which may alter content. The journal's standard [Terms & Conditions](#) and the [Ethical guidelines](#) still apply. In no event shall the Royal Society of Chemistry be held responsible for any errors or omissions in this *Accepted Manuscript* or any consequences arising from the use of any information it contains.

Revised manuscript
(CE-ART-01-2016-000151)**Structural variation of transition metal coordination polymers based on bent carboxylate and flexible spacer ligand: polymorphism, gas adsorption and SC-SC transmetallation†‡**Arun Pal,^a Santanu Chand,^a S. Senthilkumar,^b Subhadip Neogi^{*b} and Madhab C. Das^{*a}^aDepartment of Chemistry, Indian Institute of Technology Kharagpur 721302, India, E-mail: mcdas@chem.iitkgp.ernet.in^bInorganic Materials & Catalysis Division, Central Salt & Marine Chemicals Research Institute (CSIR), Bhavnagar-364002, Gujarat, India. E-mail: sneogi@csmcri.org

Abstract. Reaction of the bent dicarboxylate ligand H₂OBA (H₂OBA = 4,4'-oxybisbenzoic acid) and flexible linker 1,4-bis(3-pyridyl)-2,3-diaza-1,3-butadiene (**L**₁), under diverse reaction conditions, forms two polymorphic Co(II) coordination polymers (CPs): {[Co(OBA)(L₁)]·DMF}_n (**1**), as a three dimensional (3D) framework with pcu alpha-Po primitive cubic topology, and {[Co(OBA)(L₁)]·DMF}_n (**2**), as two dimensional (2D) structure with 6-c uninodal net topology. Gas adsorption measurements of the desolvated Co(II) CPs show negligible uptake for all gases in **1**, while **2** exhibits moderate uptake of CO₂, with good selectivity over N₂ and CH₄. With Zn(II), reaction of H₂OBA and **L**₁ produces a different 2D CP {[Zn_{0.5}(OBA)_{0.5}(L₁)_{0.5}]}_n (**3**). Finally, three isostructural Cd(II) CPs: {[Cd(OBA)(L₁)]·DMF}_n (**4**), {[Cd(OBA)(L₁)]·DEF}_n (**5**), and {[Cd(OBA)(L₁)]·DMA}_n (**6**) (DMF = N, N-dimethylformamide, DEF = N, N-diethylformamide, DMA = N, N-dimethylacetamide) are prepared that differ only in the lattice solvent molecules and show 2D structural arrangements. Interestingly, CP **4** undergoes single-crystal to single crystal (SC-SC) transmetallation reaction at room temperature, yielding isostructural {[Cu(OBA)(L₁)]·DMF}_n (**7**) that cannot be synthesized independently. Moreover, the luminescent properties of compounds **1**, **2**, **3**, **4** have been studied in the solid state at room temperature. All the complexes are characterized by elemental analysis, IR, TGA, PXRD and single crystal X-ray diffraction.

Introduction.

Coordination polymers (CPs), consisting of metal ions linked together by organic bridging ligands,¹⁻² are new class of polymeric materials that dwell between the interface of molecular coordination chemistry and material science.³ Over the past few years porous coordination polymers have drawn the attention due to their synthetic control that allows the understanding of high surface area and adjustable pore dimensions as well as promising applications in different fields such as gas storage, gas separations, magnetism, catalysis, optics, sensing, photoluminescence and many others.⁴⁻⁷ The very high adsorption behaviors, and excellent reversibility kinetics is a result of their many favorable attributes, such as reproducible and facile syntheses, high porosity, chemical modification and amenability to scale-up.⁸⁻¹⁰

Since the process of self-assembly can frequently be modulated by various external factors, such as metal source, ligands, solvents, templates, pH value, temperature, and so on, the same reactants can usually result in completely different structures because of the extreme sensitivity of self-assembly to the reaction conditions.¹¹ Among all other factors, the judicious choice of appropriate organic ligands has proven to be one of the most effective ways to manipulate versatile structures, where the length, rigidity, coordination modes, functional groups, or substituents in the organic ligands can bring about consequential effects on the final structures.¹²

The synthesis of mixed ligand CPs using polycarboxylates and N,N'-donor spacers has been established as a significant strategy to manipulate the overall structures with required functionality.¹³ Much effort has been devoted to using linear rod-like ligands (linkers) such as, 4,4'-bipyridine; pyrazine; 4,4'-azobis(pyridine); 1,2-di(4-pyridyl) ethane; 1,2-di(4-pyridyl)ethylene; 1,3-bis(4-pyridyl)propane in combination with various polycarboxylate ligands to synthesize numerous CPs ranging from 1D to 3D networks.¹⁴ Since altering of the length and functionalization of a spacer is synthetically feasible, structural diversity and variation of porosity can easily be attained by the use of flexible carboxylates with neutral linkers.¹⁵ Here, we have chosen the V-shaped 4,4'-oxybisbenzoate (OBA) as the bent carboxylate and L_1 (1,4-bis(3-pyridyl)-2,3-diaza-1,3-butadiene) as the linear spacer to construct both 2D and 3D structures by varying the reaction conditions. The pyridyl based linker can pillar the metal-carboxylate motifs into

different dimensionality to alter the structural frameworks. To this end, we report the synthesis and structures of seven CPs (**1-7**) under solvothermal conditions as well as room temperature crystallization forming different 2D layers or 3D networks. Solid state photoluminescence properties of **1, 2, 3, 4** were also investigated.

In the current work, the role of the modulators has been extended further to produce two new polymorphs (**1** and **2**) with different topology and diverse pore systems. From a fundamental point of view, the study of polymorphism in coordination chemistry is important as it allows to develop a basic understanding of the factors influencing crystal growth, such as reaction temperature, solvent system, pressure etc.¹⁶ Additionally, producing new materials through polymorphism leads to exceptional structural diversity and improved storage capacities or shape/size selective catalysis. In the case of CPs, however, there are not too many examples of polymorphism.¹⁶ Gas adsorption measurements of the desolvated Co(II) polymorphs show negligible uptake of all gases for **1**, while **2** shows moderate uptake of CO₂, with good selectivity over N₂ and CH₄, at 273K.

Interestingly, CP **4** undergoes complete transmetallation reaction to produce the Cu(II)-analogue through a single-crystal-to-single-crystal (SC-SC) fashion. The conversions of CPs to other isostructural CPs *via* the replacement of a framework metal ion (i.e., transmetallation) is very fascinating and has been documented very recently.¹⁷ However, SC-SC transmetallation is a challenging task since cleavage/ formation of coordinate bonds often leads to complete loss of structural integrity and particularly, single crystallinity. To better elucidate the exchange mechanism, investigations of the metal replacement behavior through SC-SC fashion are therefore indispensable.¹⁸

Experimental section

Materials. Co(NO₃)₂·6H₂O (Merck), Zn(NO₃)₂·6H₂O (Merck), Cd(NO₃)₂·4H₂O (Merck), Cu(NO₃)₂·3H₂O (Merck), 3-pyridinecarboxaldehyde (Sigma Aldrich), Hydrazine hydrate (Merck), 4,4'-oxybisbenzoic acid (H₂OBA) (Alfa Aesar), organic solvents (DMF, DMA, DEF) were used as obtained, without further purification.

Synthesis.

Synthesis of 1, 4-bis (3-pyridyl)-2, 3-diaza-1, 3-butadiene (L_1).

Ligand 1, 4-bis(3-pyridyl)-2, 3-diaza-1, 3-butadiene (L_1) was synthesized by adopting the procedure with slight modifications.¹⁹ 3-pyridinecarboxaldehyde (3.75 ml, 40 mmol) was dissolved in 30 ml dry ethanol. Then hydrazine hydrate (0.97 ml, 20 mmol) was added drop wise to this solution and the mixture was allowed to stir at room temperature for 24 h under the nitrogen atmosphere. The yellow precipitate thus obtained was collected and washed with cold ethanol/hexane mixture (1:1, 20 ml) and dried in high vacuum. Yield: 90% (4.75 gm). ¹H NMR (400 MHz, CDCl₃, ppm): 8.96 (s, 2 H, pyridyl), 8.69 (d, 2 H, pyridyl), 8.65 (s, 2 H, H-C=N), 8.20 (t, 2 H, pyridyl), 7.39 (q, 2 H, pyridyl). ¹³C NMR (100 MHz, CDCl₃, ppm): δ 123.9, 129.8, 135, 150.6, 152.02, 159.9 (Fig. S1, ESI). Mass (MALDI-TOF): m/z 211.457 (M+1). FT-IR (KBr pellet, cm⁻¹): 1629(s), 1588.8(s), 1480.3(s), 1417.8(s), 1305.9(s), 1227(s), 1115.1(s), 1088.8(s). Anal. Calcd for C₁₂H₁₀N₄: C, 68.57%; H, 4.76%; N, 26.67%. Found: C, 68.46%; H, 4.59%; N, 26.52%. M.P: 144⁰C.

{[Co(OBA)(L_1)]·DMF}_n, 1. A mixture of Co(NO₃)₂·6H₂O (0.1 mmol, 0.0291 gm), H₂OBA (0.1 mmol, 0.026 gm), L_1 (0.1 mmol, 0.021 gm) was dissolved in DMF (5 ml) and stirred for 1 h. Then the solution was left to stand at room temperature. Red crystals were obtained after about one month in 60% (35.9 mg) yield based on metal. Elemental analysis, Calcd: C, 58.14%; H, 4.18%; N, 11.70%. Found: C, 58.21%; H, 4.19%; N, 11.55%. FT-IR (KBr pellet, cm⁻¹): 3441(b), 3063.3(w), 2921.21(w), 2846.5(w), 1664.5(m), 1585(s), 1528(m), 1410(s), 1306.4(w), 1218.4(s), 1157.1(s), 1089.5(m), 1001.6(w), 873.6(s), 691.4(s), 657.6(m), 522.6(w).

{[Co(OBA)(L_1)]·DMF}_n, 2. A mixture of Co(NO₃)₂·6H₂O (0.1 mmol, 0.0291 gm), H₂OBA (0.1 mmol, 0.026 gm) and L_1 (0.1 mmol, 0.021 gm) and DMF (5 ml) was placed in a 15 ml Teflon-lined stainless steel vessel, heated to 110 °C for 48 h and then cooled to room temperature over 10 h. Red block crystals of **2** were obtained in 50% (29.93 mg) yield based on metal. Elemental analysis, Calcd: C, 58.14%; H, 4.18%; N, 11.70%. Found: C, 58.21%; H, 4.20%; N, 11.57%. FT-IR (KBr pellet, cm⁻¹): 3421.1(b), 3055.9(m), 2937.5(w), 2852(w), 1680.9(s), 1628(m), 1590(s), 1555(m), 1546.1(m),

1503.3(m), 1470.4(m), 1412(s), 1309.2(m), 1243.4(s), 1164.5(m), 1088.8(m), 878.29(s), 845(m), 782.89(s), 700.66(s), 654.61(s), 628.3(m), 513.2(m), 509.87(m).

$\{[\text{Zn}_{0.5}(\text{OBA})_{0.5}(\text{L}_1)_{0.5}]\}_n$, **3**. The complex **3** was synthesized similarly as **1**, except that $\text{Co}(\text{NO}_3)_2 \cdot 6\text{H}_2\text{O}$ was replaced with $\text{Zn}(\text{NO}_3)_2 \cdot 6\text{H}_2\text{O}$ (0.1 mmol, 0.030 gm). Yellow crystals of **3** were obtained after 15 days in 60% (31.91 mg) yield based on metal. Elemental analysis, Calcd: C, 58.67%; H, 3.38%; N, 10.53%. Found: C, 58.55%; H, 3.25%; N, 10.45%. FT-IR (KBr pellet, cm^{-1}): 3035.8(m), 2799.4(w), 2482.1(m), 1927.6(m), 1677.8(s), 1580(s), 1488.5(s), 1430(m), 1366.8(s), 1319.7(m), 1231.7(s), 1150.8(s), 1089.5(m), 1049.5(m), 1001.5(m), 873.6(s), 778.5(s), 684.3(s), 643.4(s), 495(m).

$\{[\text{Cd}(\text{OBA})(\text{L}_1)].\text{DMF}\}_n$, **4**. The complex **4** was synthesized similarly as **1**, except that $\text{Co}(\text{NO}_3)_2 \cdot 6\text{H}_2\text{O}$ was replaced with $\text{Cd}(\text{NO}_3)_2 \cdot 4\text{H}_2\text{O}$ (0.1 mmol, 0.031 gm). Yellow crystals of **4** were obtained after 15 days in 70% (45.63 mg) yield based on metal. **4** could also be synthesized under solvothermal condition (5 ml DMF) with similar molar ratio at 110°C for 2 days. Elemental analysis, Calcd: C, 53.38%; H, 3.83%; N, 10.74%. Found: C, 53.22%; H, 3.77%; N, 10.88%. FT-IR (KBr pellet, cm^{-1}): 3447.4(b), 3065.8(m), 2930.9(w), 2852(w), 1680.9(s), 1628(m), 1595.4(s), 1540(s), 1500(m), 1402(s), 1309.2(m), 1240.1(s), 1164.5(s), 1088.8(m), 881.58(s), 842.11(m), 782.89(s), 697.37(s), 651.32(m), 519.74(m).

$\{[\text{Cd}(\text{OBA})(\text{L}_1)].\text{DEF}\}_n$, **5**. The complex **5** was synthesized similarly as **2**, except that $\text{Co}(\text{NO}_3)_2 \cdot 6\text{H}_2\text{O}$ and DMF were replaced with $\text{Cd}(\text{NO}_3)_2 \cdot 4\text{H}_2\text{O}$ (0.1 mmol, 0.031 gm), and DEF (5 ml). Yellow crystals of **5** were obtained in 50% (34 mg) yield based on metal. Elemental analysis, Calcd: C, 54.71%; H, 4.26%; N, 10.29%. Found: C, 54.80%; H, 4.15%; N, 10.11%. FT-IR (KBr pellet, cm^{-1}): 3410(b), 3068.3(w), 2975.3(w), 2927.4(w), 1670.7(s), 1597(s), 1542 (s), 1399(s), 1299.3(w), 1245.1(s), 1164.2(m), 1102.9(w), 880.7(s), 772.3(s), 697.6(s), 650.5(m), 522.4(w).

$\{[\text{Cd}(\text{OBA})(\text{L}_1)].\text{DMA}\}_n$, **6**. The complex **6** was synthesized similarly as **1**, except that $\text{Co}(\text{NO}_3)_2 \cdot 6\text{H}_2\text{O}$ and DMF were replaced with $\text{Cd}(\text{NO}_3)_2 \cdot 4\text{H}_2\text{O}$ (0.1 mmol, 0.031 gm) and DMA (5 ml). Yellow crystals of **6** were obtained after 15 days in 30% (20 mg) yield based on metal. Elemental analysis, Calcd: C, 54.06%; H, 4.05%; N, 10.51%. Found: C, 53.93%; H, 3.91%; N, 10.44%. FT-IR (KBr pellet, cm^{-1}): 3414.3(b), 3056.2(w), 2927.3(w), 1711.6(m), 1630.7(s), 1595(s), 1539(s), 1394(s), 1231.7(m), 1150.85(m), 1096.7(w), 1008.7(m), 860.3(s), 778.5(s), 691.4(s), 637.2(m).

$\{[\text{Cu}(\text{OBA})(\text{L}_1)].\text{DMF}\}_n$, **7**. This complex is a transmetallated complex from complex **4**. Yellow crystals of **4** gradually turned into intense blue crystals of **7** when dipped in a solution of $\text{Cu}(\text{NO}_3)_2 \cdot 3\text{H}_2\text{O}$ (0.05 M) in DMF at RT for 5 days. Elemental analysis, Calcd: C, 57.70%; H, 4.15%; N, 11.61%. Found: C, 57.56%; H, 4.09%; N, 11.53%. FT-IR (KBr pellet, cm^{-1}): 3401(b), 3049.1(w), 2921.1(w), 1670.7(m), 1597(s), 1556.1(s), 1502(w), 1387(s), 1306.4(m), 1258.4(s), 1164.2(m), 1102.9(m), 1055.8(w), 873.6(m), 772.3(s), 691.4(s), 663.9(m), 495(m).

Physical Measurements. The FT-IR spectra were recorded from KBr pellets in the range of 400-4000 cm^{-1} on a Perkin-Elmer RX1 spectrophotometer. Elemental analyses (C, H, and N) were carried out on a Perkin-Elmer instrument, series II Model 2400 elemental analyzer. PXRD patterns were recorded using Cu $K\alpha$ radiation (1.5418 Å) on a Bruker D8 Advance diffractometer. Thermal analyses were performed on a Netzsch STA 449C thermal analyzer from room temperature at a heating rate of 10°C min^{-1} in nitrogen atmosphere. The luminescence spectra for the powdered solid samples were measured at room temperature on a Horiba Fluorolog Spectrophotometer. The excitation slit, as well as the emission slit were 2.5 nm. ^1H , ^{13}C -NMR spectrum was recorded using a Bruker Avance II 400 spectrometer. Mass (MALDI-TOF) spectrum was recorded using a Bruker MALDI-TOF/TOF mass spectrometer. Energy-dispersive X-ray spectroscopic data (EDX) was performed with a supra 40, Carl Zeiss Pvt. Ltd instrument. Low pressure gas adsorption measurements were performed using a static volumetric system (Micromeritics ASAP 2020) at different temperatures.

X-ray Crystallography. The crystal and refinement data for **1-7** are collected in Table 1 and Table 2. In each case, a crystal of suitable size was selected from the mother liquor and immersed in paratone oil, and then it was mounted on the tip of a glass fiber and cemented using epoxy resin. Single crystal X-ray data were collected at 100 K on a Bruker SMART APEX II CCD diffractometer using graphite-monochromated Mo-K α radiation ($\lambda = 0.71069 \text{ \AA}$). The linear absorption coefficients, scattering factors for the atoms, and the anomalous dispersion corrections were taken from International Tables for X-ray Crystallography. The data integration and reduction were processed with SAINT²⁰ software. An empirical absorption correction was applied to the collected reflections with SADABS using XPREP.²¹ The structure was solved by the direct method using SHELXTL²² and was refined on F² by full-matrix least-squares technique using the SHELXL-97²³ program package. For all the cases non-hydrogen atoms were refined anisotropically. Attempts to identify the highly disordered solvent molecules in compound **1** were failed. Instead, a new set of F² (hkl) values with the contribution from the solvent molecules withdrawn was obtained by the SQUEEZE procedure implemented in PLATON.²⁴

Table 1. Crystal data and structure refinements for complexes **1-3**.

	1	2	3
Empirical formula	C ₂₆ H ₁₈ CoN ₄ O ₅	C ₂₉ H ₂₅ CoN ₅ O ₆	C ₂₆ H ₁₈ ZnN ₄ O ₅
Formula weight	525.37	598.47	531.81
Temperature (K)	100(1)	100(1)	100(1)
Radiation	Mo-K α	Mo-K α	Mo-K α
Wavelength(λ)	0.71069 \AA	0.71069 \AA	0.71069 \AA
Crystal system	Orthorhombic	Monoclinic	Monoclinic
Space group	<i>Pnna</i>	<i>P2₁/c</i>	<i>C2/c</i>
<i>a</i> [\AA]	21.638(5)	14.556(5)	10.284(5)
<i>b</i> [\AA]	20.983(5)	12.648(5)	19.302(5)
<i>c</i> [\AA]	12.364(5)	17.312(5)	11.701(5)
α [$^\circ$]	90.00	90.00	90.00
β [$^\circ$]	90.00	110.840(5)	102.472(5)
γ [$^\circ$]	90.00	90.00	90.00
Volume[\AA^3]	5614(3)	2978.7(18)	2267.9(16)
<i>Z</i>	8	4	4
Density [Mg/m ³]	1.243	1.335	1.558
Absorption	0.650	0.625	1.131

coefficient [mm^{-1}]			
$F(000)$	2152	1236	1088
Refl. used [$I > 2\sigma(I)$]	4524	4897	2152
Independent reflections	7003	6188	2357
R_{int}	0.0696	0.0500	0.0364
Refinement method	full-matrix least squares on F^2	full-matrix least squares on F^2	full-matrix least squares on F^2
GOF	1.019	1.039	1.098
Final R indices [$I > 2\sigma(I)$]	$R_1 = 0.0569$ $wR_2 = 0.1500$	$R_1 = 0.0728$ $wR_2 = 0.2205$	$R_1 = 0.0328$ $wR_2 = 0.0897$
R indices (all data)	$R_1 = 0.0843$ $wR_2 = 0.1727$	$R_1 = 0.0884$ $wR_2 = 0.2355$	$R_1 = 0.0366$ $wR_2 = 0.0922$

Table 2. Crystal data and structure refinements for complexes 4–7.

	4	5	6	7
Empirical formula	$\text{C}_{29}\text{H}_{25}\text{CdN}_5\text{O}_6$	$\text{C}_{31}\text{H}_{29}\text{CdN}_5\text{O}_6$	$\text{C}_{30}\text{H}_{27}\text{CdN}_5\text{O}_6$	$\text{C}_{29}\text{H}_{25}\text{CuN}_5\text{O}_6$
Formula weight	651.94	679.98	665.97	603.08
Temperature (K)	100(1)	100(1)	100(1)	100(1)
Radiation	Mo-K α	Mo-K α	Mo-K α	Mo-K α
Wavelength(λ)	0.71069 Å	0.71069 Å	0.71069 Å	0.71069 Å
Crystal system	Monoclinic	Monoclinic	Monoclinic	Monoclinic
Space group	$P2_1/c$	$P2_1/c$	$P2_1/c$	$P2_1/c$
a [Å]	14.298(5)	14.261(5)	14.499(5)	14.268(5)
b [Å]	12.999(5)	13.024(5)	12.841(5)	12.993(5)
c [Å]	16.979(5)	17.038(5)	16.771(5)	16.902(5)
α [°]	90.00	90.00	90.00	90.00
β [°]	108.280(5)	108.197(5)	108.244(5)	107.945(5)
γ [°]	90.00	90.00	90.00	90.00
Volume [Å ³]	2996.5(18)	3006.3(18)	2965.5(18)	2980.9(18)
Z	4	4	4	4
Density [Mg/m^3]	1.445	1.500	1.492	1.344
Absorption coefficient [mm^{-1}]	0.777	0.778	0.787	0.781
$F(000)$	1320	1380	1352	1244
Refl. used [$I > 2\sigma(I)$]	5347	3890	3735	4441
Independent reflections	6216	4873	5192	5866
R_{int}	0.0363	0.0678	0.1040	0.0740
Refinement method	full-matrix least squares on F^2			

GOF	1.040	1.036	1.073	1.050
Final <i>R</i> indices [$I > 2\sigma(I)$]	$R_1=0.0556$ $wR_2=0.1573$	$R_1=0.0357$ $wR_2=0.0847$	$R_1=0.0561$ $wR_2=0.1355$	$R_1=0.0781$ $wR_2=0.1844$
<i>R</i> indices (all data)	$R_1=0.0638$ $wR_2=0.1641$	$R_1=0.0508$ $wR_2=0.0929$	$R_1=0.0818$ $wR_2=0.1537$	$R_1=0.1009$ $wR_2=0.2284$

Results and Discussion

Crystal structure of $\{[\text{Co}(\text{OBA})(\text{L}_1)]\cdot\text{DMF}\}_n$, (1). Single crystal X-ray study reveals that compound **1** crystallizes in the orthorhombic system with *Pnna* space group. Structural investigation shows that asymmetric unit of **1** contains one Co(II) ion, one OBA²⁻ ligand and one L₁ linker where two symmetry related Co(II) centers (Co1, Co1A) are bridged by two carboxylate groups of two OBA²⁻ ligands to form a Co₂(COO)₂ dimeric unit with a Co(II)...Co(II) separation of 4.129(9) Å (Fig. 1a). As shown in Figure 1b, each Co(II) ion adopts a distorted octahedral geometry via coordinating with four oxygen atoms (O2, O3, O4, O5) from three OBA²⁻ anions in the equatorial plane and two nitrogen atom (N3, N4) from two L₁ ligand at the axial sites. The Co–N bond lengths vary from 2.156(2) to 2.157(2) Å, while the Co–O bond distances lie within 2.0026(18)–2.223(2) Å, which are in the normal range (Table S1, ESI). Interestingly, two carboxylate groups of OBA²⁻ ligand adopt different coordination modes in **1**. While one carboxylate group adopts bidentate chelating mode, the other adopts $\mu_2\text{-}\eta^1\text{:}\eta^1$ bidentate bridging mode forming the dimeric Co(II) unit (Fig. 1a) which is also established by careful examination of asymmetric and symmetric stretching frequency of carboxylate groups in FTIR spectra (Table S2, ESI).²⁵ The bent OBA²⁻ ligand, acting as μ_3 -bridging ligands, connect the dimeric units to form corrugated 2D layers. The axially coordinated L₁ spacers connect these layers resulting in the formation of a 3D framework. A close inspection of the structure of **1** divulges that terminal pyridyl groups of L₁ are engaged in $\pi\cdots\pi$ stacking interactions (centroid-to-centroid distance of 3.916(1) Å). Moreover, two intermolecular C—H \cdots O interactions exist between the spacer and the OBA²⁻ ligand. These secondary interactions are responsible for stabilizing the overall 3D structure (Table S3, ESI). Figure 2 represents the 3-D packing diagram of **1**, showing the 1D channels of dimension 10.31 Å X 12.46 Å (considering atom to atom distance), running

along the *c* axis. The solvent composition in **1** was established from a combination of elemental analysis and TGA, which is in good agreement with the PLATON²⁴ calculated solvent-accessible volume (1294.5 Å³, 23.1 %) from the single crystal structure analysis. Furthermore, topological analysis was carried out to get more insight into the structure,²⁶ which showed that the 3D framework can be best described as a pcu alpha-Po primitive cubic topology with point symbol: {4⁴12.6³} (Fig. S2, ESI), using L₁ and OBA²⁻ ligands as linkers and dimeric Co(II) units as connectors.

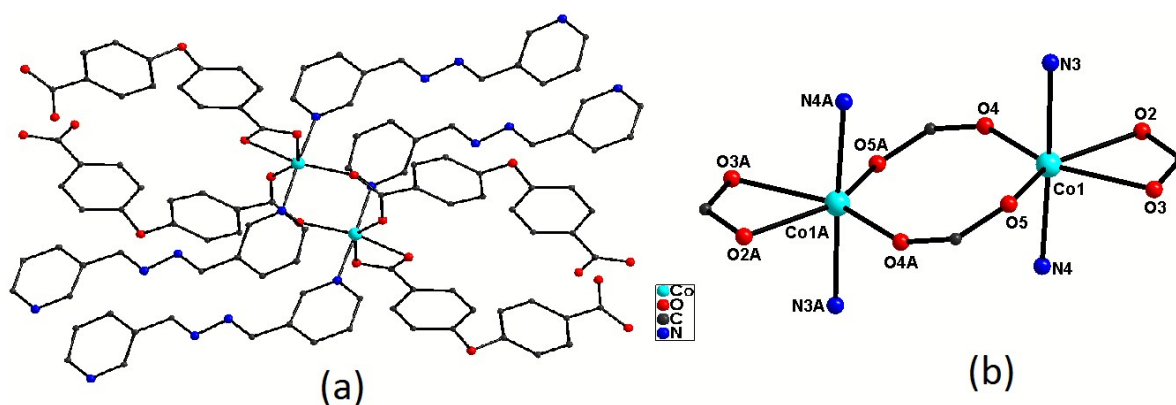
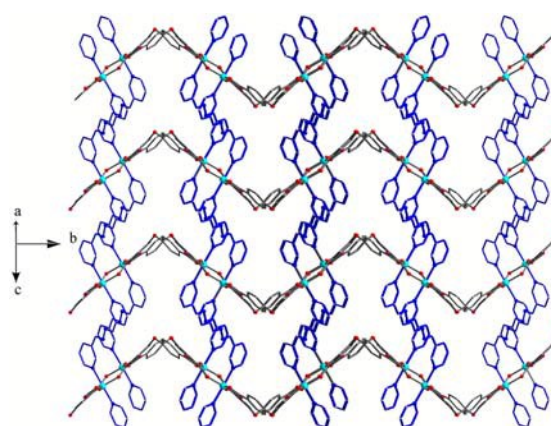


Fig. 1: (a) Coordination environment around Co metal of complex **1**, (b) Core view of complex **1** (symmetry operation (A): 0.5-x, 0.5+y, 1.5-z). H atoms are omitted for clarity.



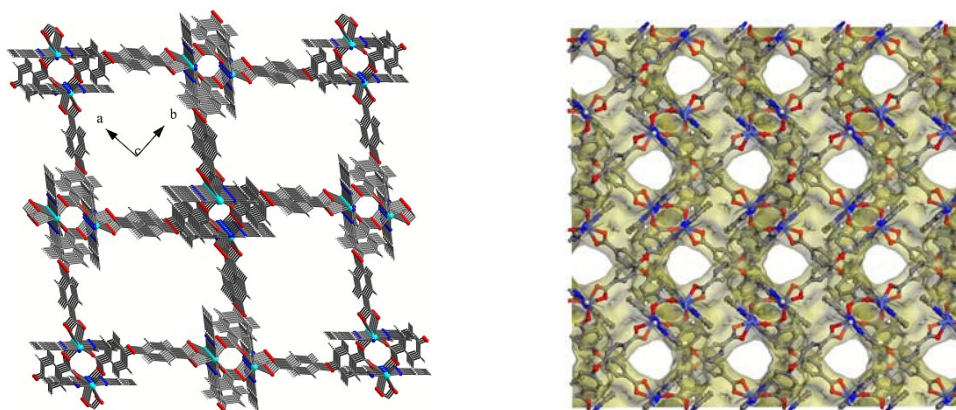


Fig. 2: View of 2D corrugated layers, joined by L_1 spacer and 3-D packing diagram of **1**, showing 1D channels running along the c axis.

Crystal structure of $\{[Co(OBA)(L_1)] \cdot DMF\}_n$ (**2**).

Interestingly, solvothermal reaction of H_2OBA , L_1 and $Co(NO_3)_2 \cdot 6H_2O$ in similar stoichiometric ratio, as used for **1**, yielded crystals with new morphology. Single crystal X-ray study reveals the formation of a different CP $\{[Co(OBA)(L_1)] \cdot DMF\}_n$ (**2**), which crystallizes in the monoclinic crystal system with $P2_1/c$ space group. Further structural investigations indicate that although, asymmetric unit of **2** exactly resembles to that of **1**, orientations of OBA^{2-} ligand changes (vide infra). A comparison of structure between **1** and **2** reveals that the coordination modes of OBA^{2-} or L_1 ligand, octahedral coordination environment around $Co(II)$ center, as well as dimeric $Co_2(COO)_2$ units are common. However, the distance between two $Co(II)$ centers in **2** (4.0430(11) Å) is found to be shorter than that in **1** (Fig. S3, ESI). Clearly, **2** exhibit polymorphism phenomena with **1**. It should be mentioned here that the significance of polymorphism in coordination polymers (framework isomerism) has recognized immense attraction,¹⁶ where this phenomenon, to our anticipation, originates due to different synthetic approach applied in this study (room temperature for **1** vs solvothermal in **2** while keeping the molar ratio of reactants and solvent system same). Most strikingly, orientation of the bent OBA^{2-} ligand with respect to planar spacer in **2** is quite distinct than that of **1**. As depicted in Figure 3, the shortest and the longest distances among the centers of aromatic rings of the spacer ligand to the centers of the aromatic moieties of OBA^{2-} ligand vary significantly in both the complexes (6.81 in **1** vs 6.94 Å in **2** and 12.28 in **1** vs 15.52 Å in **2**). Also, the

dihedral angle between the mean planes of the spacer and phenyl carboxylate at the far end of the OBA^{2-} ligand is 44.24° in **1**, which is extended to almost twice (86.0°) in **2**. Because of the different orientation of the OBA^{2-} ligand, the dimeric Co(II) units bridged by these ligands are extended in two directions giving rise to a 2D layer structure (Figure 4), rather than 3D. It should be noted that similar to **1**, weak $\pi \cdots \pi$ stacking interactions (centroid-to-centroid distance of $3.8036(8) \text{ \AA}$ compared to $3.916(1) \text{ \AA}$ in **1**) also exists among adjacent aromatic moieties of L_1 ligands in **2**. Moreover, lattice DMF molecules are engaged in $\text{C—H} \cdots \text{O}$ interactions with the OBA^{2-} ligand and pyridyl moiety of the spacer, where these weak intermolecular interactions render stability to the overall 2D structure (Table S3, ESI). Total potential solvent accessible volume is 910.7 \AA^3 per unit cell volume of 2978.7 \AA^3 (30.6%) as estimated by PLATON.²⁴ The topological analysis reveals a 6-c uninodal net topology having point symbol: $\{3^6.4^6.5^3\}$ (Fig. S4, ESI).²⁶

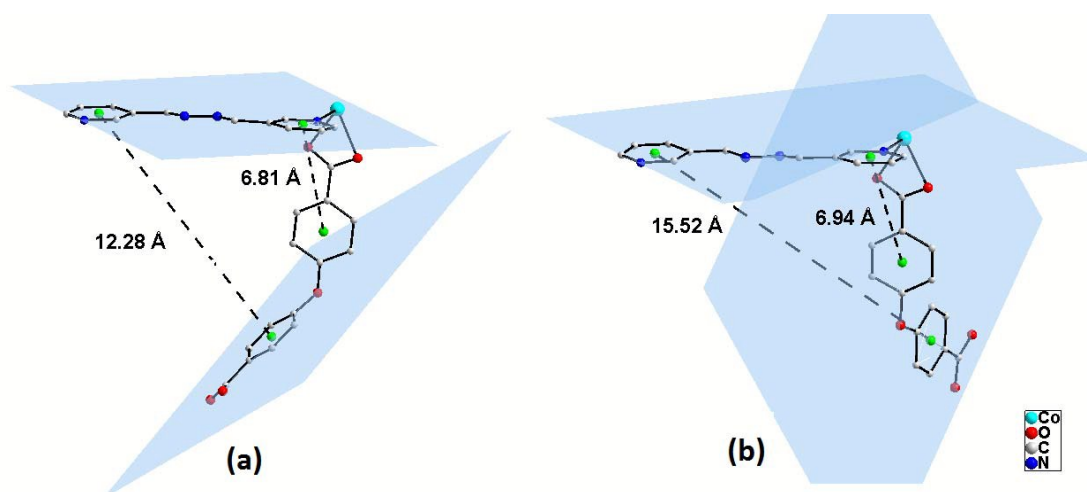


Fig. 3: Different orientations of OBA^{2-} ligand with respect to planar spacer in the asymmetric units of CP **1** (a) and CP **2** (b). The dihedral angles between the planes as shown in the figure are 44.24° in (a, for CP **1**) and 86.0° in (b, for CP **2**). H atoms are omitted for clarity.

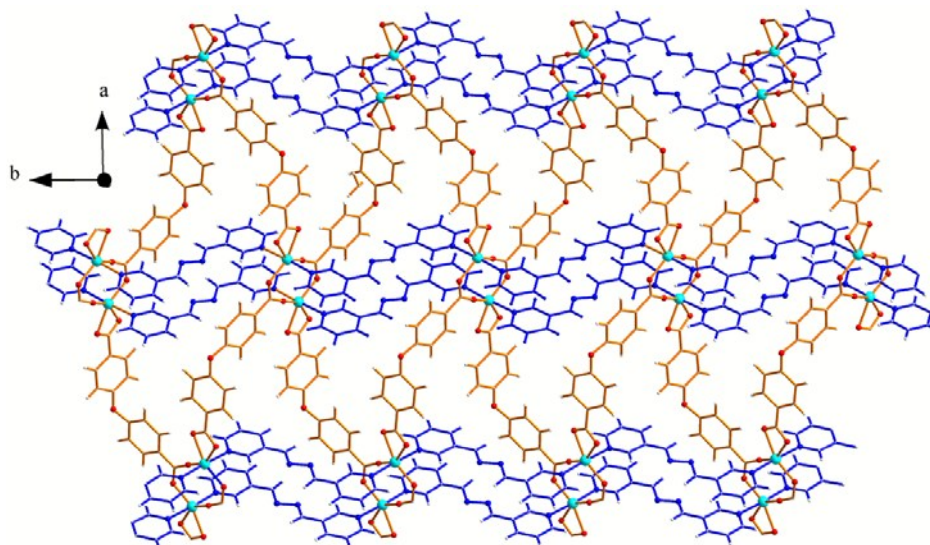


Fig. 4: Representation of 2-D packing diagram of complex **2** viewed along crystallographic *c* axis.

$\{[\text{Zn}_{0.5}(\text{OBA})_{0.5}(\text{L}_1)_{0.5}]\}_n$, (**3**). Compound **3** crystallizes in the monoclinic crystal system with the space group $C2/c$. Single crystal X-ray structure determination reveals a 2D zigzag structure. The asymmetric unit of **3** consists of a half of Zn(II) ion, half of OBA^{2-} ligand and half of L_1 spacer without any lattice solvent molecule. Figure 5 (and Fig. S5, ESI) depicts the coordination environment around Zn(II) center, adopting a highly distorted octahedral geometry surrounded by two symmetry-related nitrogen atoms from two L_1 ligands and two sets of symmetry related oxygen atoms from two OBA^{2-} ligands. The two carboxylate groups of the OBA^{2-} ligand show the bidentate chelating coordination mode (Table S2, ESI).²⁵ The Zn–N bond lengths vary from 2.288(4) to 2.326(4) Å, while the Zn–O bond lengths are from 2.308(3) to 2.620(3) Å (Table S1, ESI). The Zn–O bond length of 2.620(3) Å is longer than usual Zn–O bond lengths.²⁷ The Zn···Zn distances separated by L_1 ligand is 11.701(5) Å, while the same created by OBA^{2-} ligand approximates to 13.809(5) Å. It is worth mentioning that in contrast to the rest of the structures, where spacer L_1 adopts almost planar orientation with minimum dihedral angle between the terminal pyridyl rings (e.g. 6.15° for **1**, 6.27° for **2**, 3.04° for **4**), the pyridyl rings of spacer in **3** is severely tilted with dihedral angle between the two planes of pyridyl rings being 77.35°. Figure 6 represents the 2-D packing diagram which shows zigzag structure along the crystallographic *a* axis. This 2-D structure is further

stabilized by several intermolecular non-covalent interactions among the constituent molecules as listed in Table S3, ESI.

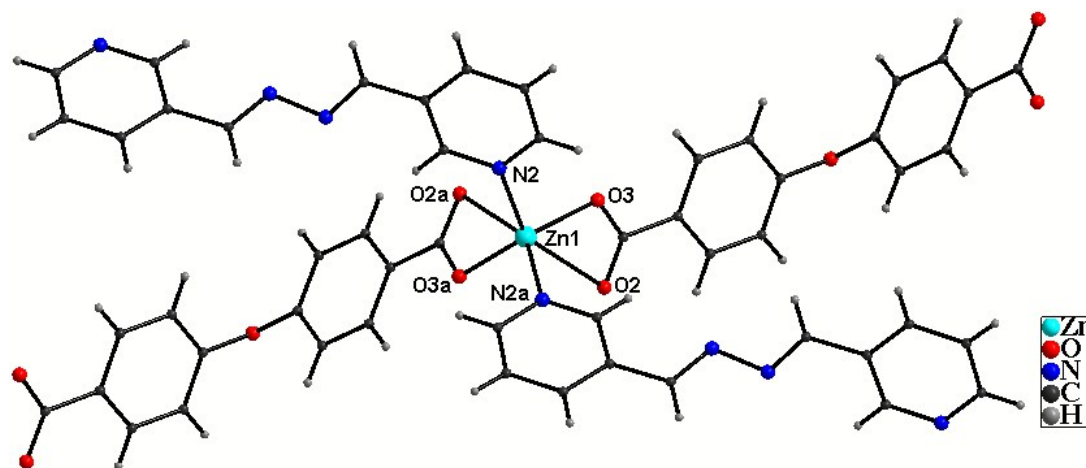


Fig. 5: Coordination environment around Zn metal of complex **3** (symmetry operation (a): $-x, y, 0.5-z$).

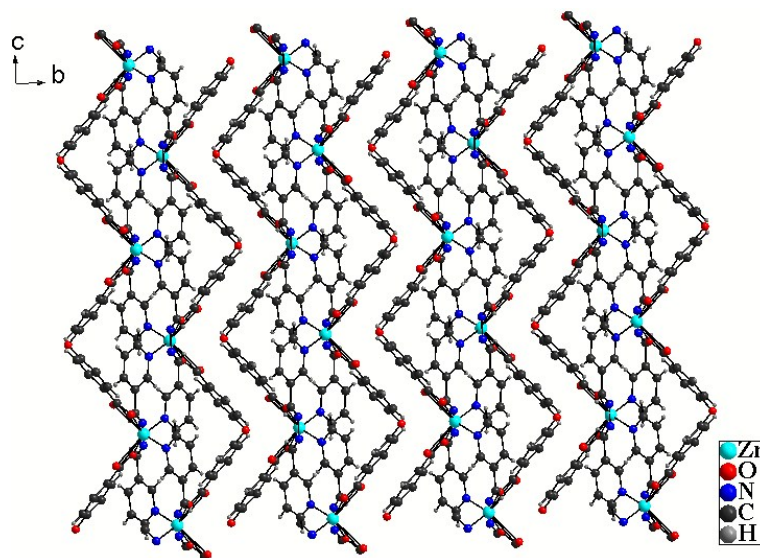


Fig. 6: Representation of 2-D packing diagram of complex **3**.

Crystal structures of $\{[Cd(OBA)(L_1)].DMF\}_n$ (4), (5), (6). Single-crystal structure analyses reveal that **4–6** are isostructural and crystallize in the monoclinic crystal system. Hence, only the structure of **4** is described in detail. The coordination environments along

with packing diagrams of other complexes and the selected bond lengths, angles and nonbonding interactions of all the complexes are listed in the Supporting Information (Fig. S8-S13, Table S1, S3, ESI). Single crystal X-ray structure determination reveals **4** as a 2D layer structure. The asymmetric unit of compound **4** consists of a one cadmium (II) ion, one OBA²⁻ ligand, one L₁ and a lattice DMF molecule. As shown in Figure 7, the Cd(II) center adopts a distorted pentagonal bipyramidal geometry surrounded by five oxygen atoms (O2, O3, O4, O4a, O5) from three different OBA²⁻ ligands in the equatorial plane and two nitrogen atoms (N1, N2) from two different L₁ ligands at the axial positions. The Cd–N bond lengths vary from 2.288(4) to 2.326(4) Å, while the Cd–O bond lengths are from 2.308(3) to 2.620(3) Å, which are in the normal range (Table S1, ESI). In complex **4**, two carboxylate groups of OBA²⁻ ligand adopt two different coordination modes: one carboxylate group adopts bidentate chelating mode and the other adopts μ_2 - η^1 : η^2 -bridging mode which are also established by careful examination of asymmetric and symmetric stretching frequency in FTIR spectra (Table S2, ESI).²⁵ Two symmetry related Cd(II) centers (Cd1, Cd1a) are bridged by two carboxylate group of OBA²⁻ ligand to form a dimeric Cd₂(COO)₂ core structure (Fig. S6, ESI). The distance between two symmetry related Cd(II) centers in this dimeric unit is 3.857(1) Å. These Cd₂(COO)₂ units are further capped with N atoms of the spacers at both ends and extended in two directions to form a layer structure (Fig. S7, ESI). Weak $\pi \cdots \pi$ stacking interactions (centroid-to-centroid distance of 3.6044(8) Å) among adjacent aromatic moieties of L₁ ligands, several other C—H \cdots O and C—H \cdots N non-covalent interactions (Table S3, ESI) among the DMF, spacer L₁ and OBA²⁻ ligand further stabilize the 2D layers.

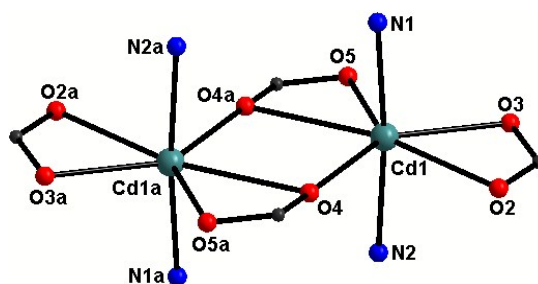


Fig. 7: Core view of complex **4** (symmetry operation (a): 1-x, -y, 2-z).

Transmetallation reaction.

Direct synthesis of the Cu(II) analogue of **4** by replacing $\text{Cd}(\text{NO}_3)_2 \cdot 6\text{H}_2\text{O}$ with $\text{Cu}(\text{NO}_3)_2 \cdot 3\text{H}_2\text{O}$, as described above, was not successful. To this end, we attempted for transmetallation reaction. When a crystal of complex **4** was dipped into the solution of $\text{Cu}(\text{NO}_3)_2 \cdot 3\text{H}_2\text{O}$ in DMF (0.05 M) at room temperature, the pale yellow crystal gradually turned into greenish blue within 5 days (Fig. S34, ESI). Crystal size, shape and morphology of the mother crystal remains unaltered throughout the exchange process, as observed from optical microscopy and diffractometer mounted single crystal photographs. This observation excludes any possibility of dissolution of the mother crystal followed by re-crystallization at the surface and growth of a new phase (Fig. S35, ESI). Moreover, the PXRD pattern of the metal exchanged material does not show any formation of a new phase and is comparable to that of **4** (Fig. S29, ESI), demonstrating that structural integrity is preserved during the metal exchange process. Complete metal-exchange was further supported by EDX of the transmetallated crystal (Fig. S36, ESI).

In spite of the fact that blue crystals are poorly diffracting, we were fortunate to obtain the single crystal X-ray structure, which showed that the transmetallated crystal has identical crystal system and structure to that of **4**, with the formula $\{[\text{Cu}(\text{OBA})(\text{L}_1)] \cdot \text{DMF}\}_n$ (**7**). As shown in Figure S14 (ESI), the Cu(II) center adopts a similar distorted pentagonal bipyramidal geometry surrounded by five oxygen atoms from three different OBA^{2-} ligands in the equatorial plane and two nitrogen atoms from two different L_1 ligands at the axial positions. The heptacoordination of Cu(II) is not so common in literature (CSD search for heptacoordination of Cu(II) gave only 87 hits (version 5.36, Nov 2014)). The Cu–N and Cu–O bond lengths are in the normal range²⁸ and almost identical to the corresponding Cd–N and Cd–O lengths of the mother crystal **4** (Table S1, ESI). As depicted in Figure 8, the distance between two symmetry related Cu(II) centers in the dimeric unit is 3.860(11) Å, which is slightly larger than the separation of Cd(II) dimer (3.857(1) Å) in **4**. However, the centroid-to-centroid distance among adjacent aromatic moieties of L_1 ligands of 3.621(8) Å in **7** is slightly larger than 3.604(8) Å in **4**. The 2D packing diagram is depicted in Fig.S15 (ESI), which unveils several non-covalent interactions (Table S3, ESI) that further stabilize the 2D layers. Since all our attempts for the direct synthesis of **7** were unsuccessful, we suggest that SC-

SC metal exchange process is the only route to obtain **7**. To our understanding, the cooperative process of simultaneous breaking of metal-ligand bonds and formation of new bonds around the incoming metal center may facilitate the formation of **7**, retaining the pristine coordination sphere, which is difficult to synthesize otherwise. However, the reverse transmetallation does not ensue for the Cu(II) exchanged product even in a concentrated DMF solution of $\text{Cd}(\text{NO}_3)_2 \cdot 6\text{H}_2\text{O}$ (1 M) under long exchange time (1 month), suggesting that the Cu(II) structure is thermodynamically more stable than the corresponding Cd(II) structure. Also, exchange behavior with Ni(II) or Co(II) metal ions for the pristine **4** exhibits no replacement under ambient condition with long exposure time (one month) or under warm condition. Thus, this metal-exchange phenomena may be correlated to the relative stabilities of the metal ligand complexes that lie in the order $\text{Co}^{\text{II}} < \text{Ni}^{\text{II}} < \text{Zn}^{\text{II}} < \text{Cu}^{\text{II}}$ in the Irving–Williams series.^{17d}

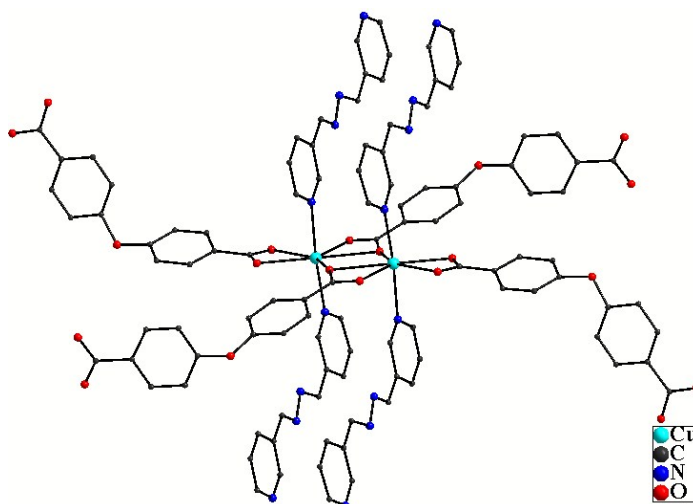


Fig. 8: Coordination environment around Cu metal of complex **7**. H atoms are omitted for clarity.

PXRD Patterns and Thermal Analyses:

In order to confirm the phase purity of these coordination polymers, the PXRD patterns were recorded for CPs **1-7**, and they were comparable to the corresponding

simulated ones (Fig. S23-S29, ESI), indicating pure phase of each bulk sample. To check the thermal stabilities of compounds **1–7**, their TGA curves were investigated under nitrogen atmosphere with a heating rate of 10°C per min (Fig. S30-S33, ESI). For compound **1**, the weight loss 11.7% occurs at 270°C, which can be attributed to the loss of lattice DMF molecule (calculated value 12.21%) and then decomposition of the structure occurs. For **2**, the weight loss of 12.40% in the temperature range 100-279°C corroborates to the loss of the lattice DMF molecule (calculated value 12.21%), followed by degradation of the framework. Compound **3** is stable up to 270°C and after that, the decomposition occurs gradually. For **4**, the weight loss 11.47% occurs at 260°C, which corresponds to the loss of uncoordinated DMF molecule (calculated value 11.21%) followed by degradation of the framework. For **5**, the weight loss 15% occurs at 280°C, which corresponds to the loss of uncoordinated DEF molecule (calculated value 14.85%) beyond which the framework starts to degrade. For **6**, weight loss 13.30% occurs at 173°C which can be attributed to the loss of lattice DMA molecule (calculated value 13.08%) and then decomposition of the framework occurs. For **7**, weight loss corresponding to the release of uncoordinated DMF molecule is 12.44% at 273°C (calculated value 12.12%) followed by decomposition of the framework. All the other weight losses beyond the temperature region of 270- 280 °C could not be elucidated in certainty. Given that the as synthesized CPs are not stable beyond this temperature region, it is expected that the *strong* metal-carboxylate interactions that tighten the backbone of the ligand to enhance the resistance to pyrolysis is absent in these CPs.²⁹ The frameworks stability of the parent complex (**4**) and the transmetallated complex (**7**) are pretty much similar to each other.

Gas Adsorption Studies:

The porous nature of **1** and **2** satisfy the essential prerequisites for gas sorption measurements. To this end, gas adsorption studies were conducted up to the relative pressure (p/p_0) of 1.0 on the activated compounds. Prior to gas adsorption measurements, CP **1** and **2** were immersed in chloroform for 5 days and heated thereafter at 100 °C for 12 h under vacuum to produce the guest-free frameworks, **1'** and **2'**, respectively. The stability of the guest free frameworks, **1'** and **2'** were confirmed by comparing the

individual PXRD patterns with that of the respective as-synthesized frameworks, which revealed perfect agreement in both the cases (Fig S39, ESI). However, compound **1'** does not adsorb any gases. Even N₂ adsorption at 77 K reveals only surface adsorption (Fig. S37, ESI). In contrast, the CO₂ adsorption experiment of **2'** showed a typical type I adsorption behavior (Figure 9a) at 273 and 298 K, confirming its microporous character. The desolvated compound starts to take up CO₂ gradually from the low-pressure region. The maximum CO₂ uptakes (1 atm) at 273 and 298 K are 57.6 and 17.2 cm³ g⁻¹, respectively. It is noteworthy that the present CO₂ sorption results are comparable with the values observed for well-known MOFs like ZIF-9, ZIF-100, other porous materials like zeolites^{1a} and activated carbon.^{30a} Furthermore, it is comparable to MOFs affording pore wall functionalized by acylamide or amide groups, and MOFs decorated by coordination-unsaturated metal sites.^{4c-4d}

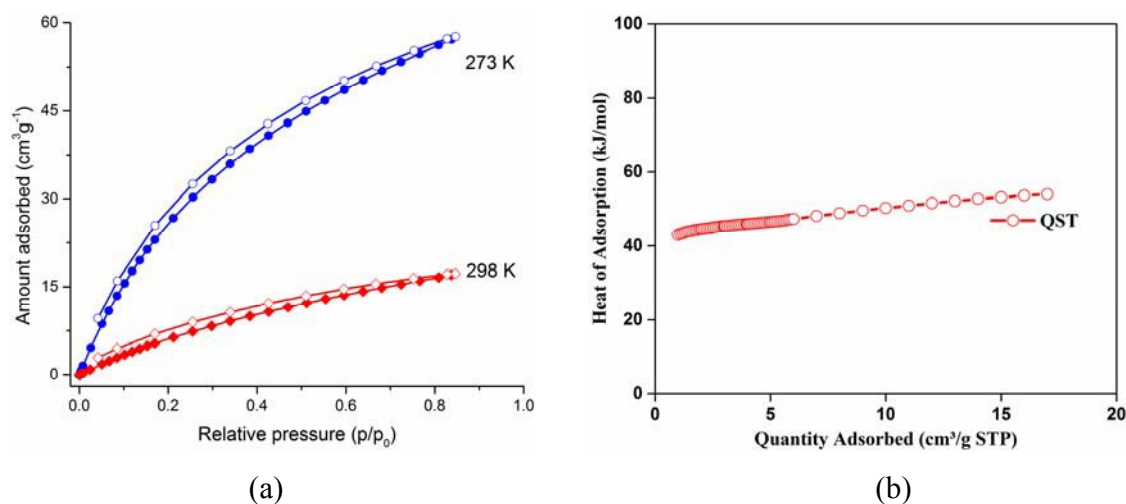


Fig. 9: (a) The CO₂ gas sorption isotherm of **2'** at 273 K (blue) and 298 K (red). Filled and open shapes indicate adsorption and desorption data points, respectively. (b) Isosteric heat of CO₂ adsorption (Q_{st}) of **2'**.

To better understand the CO₂ sorption properties, we calculated the isosteric heat of CO₂ adsorption (Q_{st}) of **2'** by the Clausius–Clayperon equation^{2c} from the isotherms obtained at 273 and 298 K. As shown in Figure 9b, the Q_{st} value for CO₂ reaches 54.0 kJ mol⁻¹ at high coverage. It should be noted that this value is significantly higher than known MOFs having –NH₂ group such as, bio-MOF-11 (45 kJ/mol), CAU-1 (48 kJ/mol), NH₂-MIL-53(Al), USO-1-Al-A (50 kJ/mol), or other MOFs like CuTATB-60, PCN-6 (35

kJ/mol), HKUST-1 (35 kJ/mol), IRMOF-1, MOF-5 (34 kJ/mol), MIL-53(Cr) (32 kJ/mol), NOTT-140 (25 kJ/mol) and UCMC-1 (12 kJ/mol). Such a high value implies that the azo moieties of pyridine linkers inside the framework are involved in strong intermolecular interactions with the adsorbed CO₂ molecules. Presumably, the slight hysteresis observed for CO₂ adsorption isotherm can be correlated with this large Q_{st} value. To further explore the potential properties of **2'** on gas separation under ambient conditions, the adsorption isotherms of CH₄ and N₂ were measured at 273 K. As shown in Figure 10, N₂ molecules did not diffuse into the pores. However, CH₄ gas molecules, having a reasonable polarizability ($25.93 \times 10^{-25} \text{ cm}^3$), enter only moderately (6.8 cc/g at 273 K and up to 1 bar) into the pore. In sharp contrast, the high quadrupole moment and polarizability of CO₂ ($13.4 \times 10^{-40} \text{ C m}^2$ and $26.3 \times 10^{-25} \text{ cm}^3$, respectively)^{2d} induce better interaction with the channels and interior wall of the CP, composed of basic azo functionalities. These interactions should be the crucial factors for superior CO₂ adsorption over other gases.

The significant challenge regarding gas separation under ambient conditions, plus the favorable distinguishing adsorption behavior of the material prompted us to examine the selective CO₂ capture ability over N₂ and CH₄ gases at 273 K. The selectivity (S) for adsorption of CO₂ over other gases was calculated from the single-component isotherm data. For CO₂ capture, this value typically reports the ratio of the adsorbed amount of CO₂ at 0.15 bar to the adsorbed amount of other gases at 0.75 bar; the value is normalized for the pressures chosen, according to equation: $S = (q_{\text{CO}_2}/q_o)/(p_{\text{CO}_2}/p_o)$, where q is the amount adsorbed and p is the relative pressure ($o = \text{Other gases}$).^{2e}

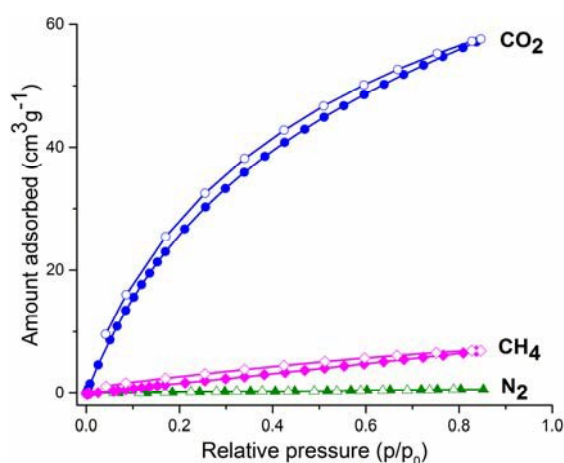


Fig. 10: The CO₂ (blue), CH₄ (pink) and N₂ (green) adsorption of **2'** at 273 K. Filled and open shapes indicate adsorption and desorption data points respectively.

The CO₂ selectivity over N₂ and CH₄ are found to be 207.2 and 17.5 respectively. Though, numerous MOFs with significant CO₂ uptake have been reported, only limited examples of porous MOFs are known that exhibit CO₂/N₂ selectivity over 200.^{30b} The high selectivity value suggest that **2'** may find potential applications for selective CO₂ capture from flue gas. Although, the CO₂/CH₄ selectivity for **2'** at 273 K, is lower than CO₂/N₂ selectivity, the value is comparable to some polyimide networks or ZIFs.^{4b, 30c}

Photoluminescence Properties:

Luminescent compounds are currently of great interest because of their various applications in chemical sensors, photochemistry and electroluminescence display. Many studies have shown that coordination polymers with cobalt, zinc, cadmium ions exhibit photoluminescence properties.³¹ To this end, luminescence properties of compound **1-4** as well as free ligands **L₁** and H₂OBA were studied in the solid state at room temperature under the same experimental conditions. The emission peaks of **L₁** and H₂OBA were observed at 476 nm and 463 nm upon excitation at 260 nm and 320 nm respectively (Fig. S38, ESI). These emissions are due to intra-ligand $\pi^* \rightarrow n$ or $\pi^* \rightarrow \pi$ charge transitions of **L₁** and H₂OBA.^{31c} The CPs **1** and **2** display broad band with the main peak at 450 nm, 445 nm and the shoulder peak at 370 nm, 363 nm upon excitation at 330 nm and 320 nm respectively which might be caused by the mixture characteristic of intra-ligand charge transitions of **L₁** and H₂OBA (Fig. 11). The emission results of **1** and **2** are the indication of close relationship of photoluminescent behavior with the coordination environment around the metal ions.^{31d} The complex **3** exhibits emission at 362 nm as shoulder peak and at 466 nm as main peak upon excitation at 330 nm which may be assigned to the mixture characteristic of intra-ligand charge transitions of **L₁** and H₂OBA (Fig. 11). The emission band of compound **4** appears in 477 nm upon excitation at 320 nm which is similar to that of free H₂OBA, which can be assigned to the intra-ligand charge transition of H₂OBA (Fig. 11). The compound **4** exhibits a small red-shift (14 nm) with respect to

free H₂OBA ligand, which may be attributed to the metal-ligand coordination interactions.

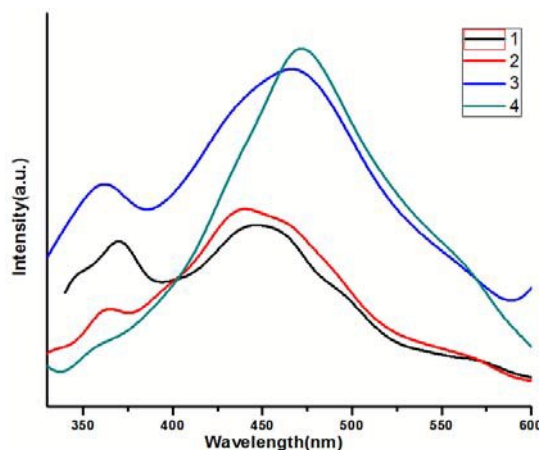


Fig. 11: Solid-state photoluminescent spectra of coordination polymers **1 - 4**.

Summary:

In summary, self-assembly of a V-shaped organic linker and a flexible *N, N'*-spacer with different transition metal ions leads to the formation of seven new complexes as two or three dimensional coordination polymers. Interestingly, using similar stoichiometric ratio of the reactants, variation of the synthetic conditions (room temperature vs. solvothermal reaction) leads to two different coordination polymers with varying dimensionalities (two and three dimension) that exhibit polymorphism phenomenon. Furthermore, the yellow crystal of Cd(II) CP undergoes single-crystal to single-crystal transmetallation reaction to produce isostructural Cu(II) CP under ambient conditions. Although, SC-SC replacement of solvent molecules and organic linkers have much been studied in CPs, only a handful example exists on metal exchange process. Metal exchange in coordination polymers leads to improved catalytic and gas storage properties and allow obtaining those structures that cannot be synthesized by *de novo* route. The CPs **4-6** are isostructural and only differ in lattice solvent molecules. All the CPs are produced in pure phase during their bulk synthesis and are moderately thermally stable. Gas adsorption measurements of the desolvated Co(II) CP-**2** shows moderate uptake of CO₂, with good selectivity over N₂ and CH₄, at 273K. CPs **1-4** exhibit normal luminescence properties as expected.

† CCDC reference numbers 1446366-1446372. For crystallographic data in CIF or other electronic format see DOI:

‡**Electronic supplementary information (ESI) available:** X-ray crystallographic files in CIF format for the structure determination of CPs **1-7**, additional figures, tables for selected bond length and bond angle, non-bonding interactions. See DOI:

Acknowledgements.

We gratefully acknowledge the financial support received from ISIRD-SRIC, IIT Kharagpur and a JRF (UGC) to A. P. CSIR-CSMCRI Communication No. 011/2016. We thank Dr. Susan Sen, Kyoto University for helpful discussion.

References.

1. (a) R. Banerjee, A. Phan, B. Wang, C. Knobler, H. Furukawa, M. O’Keeffe and O. M. Yaghi, *Science*, 2008, **319**, 939; (b) H. C. Zhou, J. R. Long and O. M. Yaghi, *Chem. Rev.*, 2012, **112**, 673; (c) P. Deria, J. E. Mondloch, O. Karagiari, W. Bury, J. T. Hupp and O. K. Farha *Chem. Soc. Rev.*, 2014, **43**, 5896; (d) S. R. Batten, S. M. Neville and D. R. Turner, *Coordination Polymers: Design, Analysis and Application*, 2008, 313.
2. (a) S. Kitagawa, R. Kitaura and S. Noro, *Angew. Chem., Int. Ed.*, 2004, **43**, 2334; (b) P. Kanoo, G. Mostafa, R. Matsuda, S. Kitagawa and T. K. Maji, *Chem. Commun.*, 2011, **47**, 8106; (c) S. S. Kaye and J. R. Long, *J. Am. Chem. Soc.* 2005, **127**, 6506; (d) A. Jarad, J. A. Mason, K. Sumida, Z. R. Herm, R. Krishna and J. R. Long, *Energy Environ. Sci.* 2011, **4**, 3030; (e) T. M. McDonald, D. M. D’Alessandro, R. Krishna and J. R. Long, *Chem. Sci.* 2011, **2**, 2022.
3. (a) D. Bradshaw, A. Garai and J. Huo, *Chem. Soc. Rev.*, 2012, **41**, 2344; (b) S. -Y. Zhang, L. Wojtas and M. J. Zaworotko, *J. Am. Chem. Soc.*, 2015, **137**, 12045.
4. (a) J.-R. Li, J. Sculley and H. C. Zhou, *Chem. Rev.*, 2012, **112**, 869; (b) R. Banerjee, H. Furukawa, D. Britt, C. Knobler, M. O’Keeffe and O. M. Yaghi, *J. Am. Chem. Soc.* 2009, **131**, 3875; (c) J. B. Lin, W. Xue, J. P. Zhang and X. M. Chen, *Chem. Commun.*, 2011, **47**, 926; (d) K. C. Stylianou, J. E. Warren, S. Y. Chong, J. Rabone, J. Bacsá, D. Bradshaw and M. J. Rosseinsky, *Chem. Commun.*, 2011, **47**, 3389.

5. (a) L. E. Kreno, K. Leong, O. K. Farha, M. Allendorf, Richard P. Van Duyne and J. T. Hupp, *Chem. Rev.* 2012, **112**, 1105; (b) Z. Hu, B. J. Deibert and J. Li *Chem. Soc. Rev.*, 2014, **43**, 5815; (c) R. Vaidhyanathan, S. S. Iremonger, K. W. Dawson and G. K. H. Shimizu, *Chem. Commun.*, 2009, **45**, 5230.
6. (a) O. Evans and W. B. Lin, *Acc. Chem. Res.*, 2002, **35**, 511; (b) M. D. Allendorf, C. A. Bauer, R. K. Bhakta and R. J. T. Houk, *Chem. Soc. Rev.*, 2009, **38**, 1330; (c) L. Carlucci, G. Ciani and D. M. Proserpio, *CrystEngComm*, 2003, **5**, 269.
7. (a) M. P. Suh, H. J. Park, T. K. Prasad and D.-W. Lim, *Chem. Rev.*, 2012, **112**, 782; (b) R. B. Getman, Y.-S. Bae, C. E. Wilmer and R. Q. Snurr, *Chem. Rev.*, 2012, **112**, 703; (c) Y. He, W. Zhou, G. Qian and B. Chen, *Chem. Soc. Rev.*, 2014, **43**, 5657; (d) Y. Cui, Y. Yue, G. Qian and B. Chen, *Chem. Rev.*, 2012, **112**, 1126.
8. (a) T. Yamada, K. Otsubo, R. Makiura and H. Kitagawa, *Chem. Soc. Rev.*, 2013, **42**, 6655; (b) M. Sadakiyo, T. Yamada, K. Kato, M Takata and H. Kitagawa *Chem. Sci.*, 2016, **7**, 1349; (c) M. Yoon, R. Srirambalaji and K. Kim, *Chem. Rev.*, 2012, **112**, 1196.
9. (a) B. Manna, S. Mukherjee, A. V. Desai, S. Sharma, R. Krishna and S. K. Ghosh, *Chem. Commun.*, 2015, **51**, 15386; (b) A. Karmakar, A. V. Desai and S. K. Ghosh, *Coord. Chem. Rev.* 2016, **307**, 313; (c) U. P. Singh, S. Narang, P. Pachfule and R. Banerjee, *CrystEngComm*, 2014, **16**, 5012; (d) S. Saha, G. Das, J. Thote and R. Banerjee, *J. Am. Chem. Soc.*, 2014, **136**, 14845.
10. (a) M. Eddaoudi, D. F. Sava, J. F. Eubank, K. Adil and V. Guillerme, *Chem. Soc. Rev.*, 2015, **44**, 228; (b) S. Sanda, S. Parshamoni, S. Biswas and S. Konar, *Chem. Commun.*, 2015, **51**, 6576; (c) M. C. Das and P. K. Bharadwaj, *J. Am. Chem. Soc.* 2009, **131**, 10942; (d) M. Kurmoo, *Chem. Soc. Rev.* 2009, **38**, 1353.
11. (a) H. Y. Li, L. H. Cao, Y. L. Wei, H. Xu and S. Q. Zang, *CrystEngComm*, 2015, **17**, 6297; (b) L. Zhou, Y.-S. Xue, Y. Xu, J. Zhang and H.-B. Du, *CrystEngComm*, 2013, **15**, 7315.
12. (a) D. Kim and M. S. Lah, *CrystEngComm*, 2013, **15**, 9491; (b) G. S. Papaefstathiou, T. Friscic and L. R. MacGillivray, *J. Am. Chem. Soc.*, 2005, **127**, 14160.
13. (a) R. Matsuda, R. Kitaura, S. Kitagawa, Y. Kubota, T. C. Kobayashi, S. Horike and M. Takata, *J. Am. Chem. Soc.*, 2004, **126**, 14063; (b) H. S. Choi and M. P. Suh,

Angew. Chem., Int. Ed., 2009, **48**, 6865 ; (c) S. Sengupta, S. Ganguly, A. Goswami, P. K. Sukul and R. Mondal, *CrystEngComm*, 2013, **15**, 8353.

14. (a) X. Li, R. Cao, D. Sun, W. Bi, Y. Wang, X. Li and M. Hong, *Cryst. Growth Des.*, 2004, **4**, 775; (b) S. Mohapatra and T. K. Maji, *Dalton Trans.*, 2010, **39**, 3412; (c) X. Duan, Q. Meng, Y. Su, Y. Li, C. Duan, X. Ren and C. Lu, *Chem. – Eur. J.*, 2011, **17**, 9936.

15. (a) C. N. R. Rao, S. Natarajan, and R. Vaidhyanathan, *Angew. Chem. Int. Ed.*, 2004, **43**, 1466; (b) T. K. Maji, K. Uemura, H.-C Chang, R. Matsuda, S. Kitagawa, *Angew. Chem.*, 2004, **116**, 3331.

16. (a) G. -X. Liu, H. Xu, H. Zhou, S. Nishihara and X.-M. Ren, *CrystEngComm*, 2012, **14**, 1856; (b) B. Chen, F. R. Fronczek and A. W. Maverick, *Chem. Commun.*, 2003, 2166; (c) V. Bon, I. Senkowska, I. A. Baburin and S. Kaskel, *Cryst. Growth Des.*, 2013, **13**, 1231.

17. (a) S. Huang, X. Li, X. Shi, H. Hou and Y. Fan, *J. Mater. Chem.*, 2010, **20**, 5695; (b) L. Mi, H. Hou, Z. Song, H. Han and Y. Fan, *Chem.–Eur. J.*, 2008, **14**, 1814; (c) M. Dinca and J. R. Long, *J. Am. Chem. Soc.*, 2007, **129**, 11172; (d) T. K. Pal, S. Neogi and P. K. Bharadwaj, *Chem. –Eur. J.* 2015, **21**, 16083; (e) S. Sen, S. Neogi, K. Rissanen and P. K. Bharadwaj, *Chem. Commun.*, 2015, **51**, 3173.

18. (a) S. Das, H. Kim and K. Kim, *J. Am. Chem. Soc.*, 2009, **131**, 3814; (b) G. Mukherjee and K. Biradha, *Chem. Commun.*, 2012, **48**, 4293; (c) R. Medishetty, T. T. S. Yap, L. L. Koh and J. J. Vittal, *Chem. Commun.*, 2013, **49**, 9567. (d) H. Aggarwal, P. M. Bhatt, C. X. Bezuidenhout and L. J. Barbour, *J. Am. Chem. Soc.* 2014, **136**, 3776; (e) H. Aggarwal, P. Lama and L. J. Barbour, *Chem. Commun.*, 2014, **50**, 14543.

19. Y.-B. Dong, M. D. Smith, R. C. Layland, and H.C. Loye, *Chem. Mater.* 2000, **12**, 1156.

20. SAINT+, 6.02ed, Bruker AXS, Madison, WI, 1999.

21. XPREP, 5.1 ed. Siemens Industrial Automation Inc., Madison, WI, 1995.

22. G. M. Sheldrick, *SHELXTL™ Reference Manual*: version 5.1, Bruker AXS, Madison, WI, 1997.

23. G. M. Sheldrick, *SHELXL-97, Program for Crystal Structure Refinement*, University of Göttingen, Göttingen, Germany, 1997.

24. Platon Program: A. L. Spek, *Acta Crystallogr., Sect. A* 1990, **46**, 194.
25. (a) A. Patra, T. K. Sen, R. Bhattacharyya, S. K. Mandal and M. Bera, *RSC Advances*, 2012, **2**, 1774; (b) M. Bera, A. B. S. Curtiss, G. T. Musie and D. R. Powell, *Inorg. Chem.* 2012, **51**, 12093; (c) V. Zelenak, Z. Vargova and K. Gyoryova, *Spectrochimica Acta Part A*, 2007, **66**, 262; (d) G. S. Groenewold, W. A. de Jong, J. Oomens and M. J. V. Stipdonk, *J. Am. Soc. Mass Spectrom.*, 2010, **21**, 719; (e) M. C. Das, S. K. Ghosh, E. C. Sañudo and P. K. Bharadwaj, *Dalton Trans.*, 2009, 1644.
26. V. A. Blatov, IUCr CompComm Newsletter, 2006, vol. 7, p. 4; <http://www.topos.ssu.samara.ru>.
27. (a) L. Wang, W. You, W. Huang, C. Wang and X. Z. You, *Inorg. Chem.* 2009, **48**, 4295; (b) A. L. Cheng, N. Liu, Y. F. Yue, Y.W. Jiang, E. Q. Gao, C.H. Yan and M. Y. He, *Chem. Commun*, 2007, 407.
28. (a) F. L. Hu, S. L. Wang, H. X. Li, B. Wu and J. P. Lang, *Inorg.Chem.Commun.*, 2014, **47**, 75; (b) F. Valach, R. Grobelny, T. Glowiak, J. Mrozinski, V. Lukes and Z. Blahova, *Journal of Coordination Chemistry*, 2010, **63**, 1645; (c) W. -J. Hu, L. -Q. Liu, M. -L. Ma, X. -L. Zhao, Y. A. Liu, X. -Q. Mi, B. Jiang and K. Wen, *Inorg. Chem.* 2013, **52**, 9309; (d) C. Dey and R. Banerjee, *ChemPhysChem*, 2013, **14**, 1009.
29. (a) H. -L. Jiang, N. Tsumori and Q. Xu, *Inorg. Chem.* 2010, **49**, 10001; (b) Y. Li, G. Xu, W. -Q. Zou, M. -S. Wang, F. -K. Zheng, M. -F. Wu, H. -Y. Zeng, G. -C. Guo, and J. -S. Huang, *Inorg. Chem.* 2008, **47**, 7945.
30. (a) S. Sircar, T. C. Golden and M. B. Rao, *Carbon*, 1996, **34**, 1; (b) K. Sumida, D. L. Rogow, J. A. Mason, T. M. McDonald, E. D. Bloch, Z. R. Herm, T. -H. Bae and J. R. Long, *Chem. Rev.*, 2012, **112**, 724; (c) G. Li and Z. Wang, *Macromolecules*, 2013, **46**, 3058.
31. (a) J. Guo, J. F. Ma, J. J. Li, J. Yang and S. X. Xing, *Cryst. Growth Des.* 2012, **12**, 6074; (b) Y. Guo, X. Feng, T. Han, S. Wang, Z. Lin, Y. Dong and B. Wang, *J. Am. Chem. Soc.* 2014, **136**, 15485; (c) Z.-Q. Shi, Y.-Z. Li, Z.-J. Guo and H. -G. Zheng, *Cryst. Growth Des.* 2013, **13**, 3078; (d) C. Xu, L. Li, Y. Wang, Q. Guo, X. Wang, H. Hou and Y. Fan, *Cryst. Growth Des.* 2011, **11**, 4667; (e) S. Su, C. Qin, Z. Guo, H. Guo, S. Song, R. Deng, F. Cao, S. Wang, G. Li and H. Zhang, *CrystEngComm*, 2011, **13**, 2935.

Graphical Abstract

Structural variation of transition metal coordination polymers based on bent carboxylate and flexible spacer ligand: polymorphism, gas adsorption and SC-SC transmetallation

Arun Pal, Santanu Chand, S. Senthilkumar, Subhadip Neogi and Madhab C. Das

Seven new coordination polymers have been synthesized and characterized by EA, IR, TGA, PXRD and SC-XRD. Polymorphism, SC-SC transmetallation and gas sorption properties have been studied.

